Ultraviolet-C Vertical-Cavity Surface-Emitting Lasers with Precise Cavity Length Control

LASER & PHOTONICS REVIEWS
www.lpr-journal.org

Ultraviolet-C Vertical-Cavity Surface-Emitting Lasers with Precise Cavity Length Control

Estrella Torres, Joachim Ciers, Nelson Rebelo, Filip Hjort, Michael A. Bergmann, Sarina Graupeter, Johannes Enslin, Giulia Cardinalli, Tim Wernicke, Michael Kneissl, and Åsa Haglund*

In vertical-cavity surface-emitting lasers (VCSELs), the cavity length defines the resonance wavelength, which is directly related to the laser detuning, that is, the difference between resonance wavelength and gain peak. A low detuning maximizes the modal gain leading to a reduction of the threshold. Therefore, controlling the cavity length of VCSELs is of great importance. Here optically pumped ultraviolet-C (wavelength $\leq$ 280 nm) VCSELs with precise cavity length control are demonstrated. The VCSEL structure is formed by an AlN cavity with 5 × $Al_{0.40}Ga_{0.60}/Al_{0.70}Ga_{0.30}N$ quantum wells and a top HfO_2 spacer layer with dielectric SiO_2/HfO_2 distributed Bragg reflectors on both sides of the cavity. To access the N-face side of the cavity, a new methodology referred to as photo-assisted electrochemical etching is employed for substrate removal. Across a 0.9 mm × 1.2 mm area, the lasing wavelength varies a maximum of 1.17 nm between different UVC VCSELs, exhibiting threshold pump power densities from 0.7 MW/cm^2 to 3.7 MW/cm^2 and detuning values between 0 to 2 nm. The results show that VCSELs with a cavity length variation lower than 1% can be obtained with this technology.

1. Introduction

Compact, efficient, long lifetime, and low-cost ultraviolet-C (UVC) lasers are in demand for applications in water, air, and surface disinfection,[1] sensing,[2] micro-processing,[3] and optical communication.[4] To date, the commercially available UVC lasers are excimer and solid-state lasers that are bulky, expensive, and have low efficiency. Laser diodes such as edge-emitting lasers (EELs) or vertical-cavity surface-emitting lasers (VCSELs) are an interesting alternative due to their compactness, lower price, and higher conversion efficiencies. Both EELs and VCSELs have proven their potential in the mature GaAs-based and InP-based materials.[5,6] When it comes to the UV, only electrically injected UV EELs have been demonstrated, in the UVB under pulsed operation[7] and in the UVC under continuous wave operation.[8] In contrast, electrically injected UV VCSELs have not yet been demonstrated. These devices are of great interest due to their advantages compared to EELs such as their circular-symmetric low-divergent output beams, two-dimensional (2D) integration capability, lower threshold current, and high modulation frequencies at low currents due to their reduced active region volume.[5]

However, UV AlGaN-based laser diodes are still in their infancy due to a number of challenges with the III-nitride material system, such as the development of templates with low threading dislocation density (TDD) and the p-doping difficulty in AlGaN layers. Moreover, process technology challenges are the result of the limited amplification rate per round trip in VCSEL, approximately 1% in GaN-based VCSELs,[9] which demands highly reflective distributed Bragg reflectors (DBRs), smooth surfaces, optical and electrical confinement, and transparent p-side ohmic contacts to minimize losses. For example, highly reflective mirrors in optically pumped UVB and UVC VCSELs have only been achieved by employing dielectric SiO_2/HfO_2 DBRs. A 10-pair dielectric DBR with a measured peak reflectivity of 99.23% at 320 nm was used in UVB VCSELs,[10,11] while a 15.5-pair DBR with 97.7% of reflectivity at 276 nm in UVC VCSELs.[12,13] However, VCSELs with all-dielectric DBRs require substrate removal techniques to access the N-face surface of the device. To address this challenge, Zheng et al.[12] employed laser lift-off to remove the substrate combined with chemical mechanical polishing to reduce the surface roughness of the exposed N-face surface. Even

E. Torres, J. Ciers, N. Rebelo, F. Hjort, M. A. Bergmann, Å. Haglund
Department of Microtechnology and Nanosciense
Chalmers University of Technology
41296 Gothenburg, Sweden
E-mail: estrella@chalmers.se
S. Graupeter, J. Enslin, G. Cardinalli, T. Wernicke, M. Kneissl
Institute of Solid State Physics
Technische Universität Berlin
10623 Berlin, Germany
J. Enslin, M. Kneissl
Ferdinand-Braun-Institut (FBH)
12489 Berlin, Germany

The ORCID identification number(s) for the author(s) of this article can be found under https://doi.org/10.1002/lpor.202402203

DOI: 10.1002/lpor.202402203

though the chemical mechanical polishing resulted in an N-face surface with a root-mean-square (RMS) down to 0.96 nm over 10 × 10 μm^2, the cavity length of a square mesa with a 200 μm side varied from 140 nm to 700 nm. This large cavity length variation is undesirable in VCSELs since the cavity length defines the resonance wavelength, and thereby the detuning between the resonance wavelength and gain peak, which greatly affects modal gain and the lasing threshold. Cardinali et al.[11] studied this impact of the cavity length influence on the threshold pump power density in 2.5λ cavity UVB VCSELs, and found that a physical cavity length variation of ≈10 nm led to an increase in threshold pump power density of a factor of 10 highlighting the importance of cavity length control in VCSEL structures.

A substrate removal technique that can provide cavity length control and potentially smooth as-etched N-face surfaces is electrochemical etching.[10,11] Electrochemical etching oxidizes and dissolves a sacrificial layer by applying a bias voltage between the sample with the sacrificial layer exposed to the electrolyte, and the reference electrode. At the semiconductor/electrolyte junction, a tunneling process drives the etching of the sacrificial layer and hence releasing the device membrane from the template.[14,15] Since this process is based on tunneling, electrochemical etching is selective with the semiconductor band gap, n-doping concentration, and the applied voltage, favoring the etching of more heavily doped layers with lower bandgap. This technology has been proven compatible with the fabrication of UVB VCSELs[10,11] providing smoothly etched N-face surfaces and good cavity length control. Furthermore, thin-film flip-chip UVB light-emitting diodes (LEDs)[16] and resonant-cavity UVB LEDs[17] including heavily doped tunnel junctions have been realized by employing this substrate removal technique. However, for UVC devices, higher Al composition (Al > 40%) is needed for the device and sacrificial layer that hampers the electrochemical etching due to the higher bandgaps and lower free carrier concentrations of those layers. In theory, these UVC sacrificial layers could be completely etched by applying just higher voltages.[14] However, our experimental investigation showed that even at ≈120 V, a complete etch of the sacrificial layer was not reached, and the risk of destroying the devices by parasitic etching at those very high voltages increased drastically. This problem was overcome by the combination of electrochemical etching with the generation of photo-excited carriers in the sacrificial layer by employing an external UVC light source which emission is mainly absorbed in the sacrificial layer. We refer to this new methodology as photo-assisted electrochemical etching (P-ECE). In this work, we used this methodology of P-ECE to remove the high-Al-containing sacrificial layer, lift-off the active AlGaN layers, and fabricate optically pumped UVC VCSELs. Another benefit of P-ECE is also a reduced bias voltage for complete etching while keeping the cavity length control, smooth surfaces, and high etch rates typical of electrochemical etching.

2. Results and Discussion

The UVC VCSEL structure consists of a 10λ AlN cavity with 5 × $Al_{0.40}Ga_{0.60}N/Al_{0.70}Ga_{0.30}N$ quantum wells (QWs) surrounded by 40 nm $Al_{0.70}Ga_{0.30}N$ barriers. The structure is grown on top of a stack of layers for lift-off purposes composed of an 18 nm n^{++}-$Al_{0.45}Ga_{0.55}N$ sacrificial layer, a 280 nm n-$Al_{0.76}Ga_{0.24}N$ etch block layer, and an 1138 nm n^{+}-$Al_{0.76}Ga_{0.24}N$ current spreading layer. The Si doping concentration of the sacrificial layer is 4 × 10^{19} cm^{-3}, etch block layer 2.4 × 10^{17} cm^{-3}, and current spreading layer is 5 × 10^{17} cm^{-3}. The device fabrication is depicted in the Process Flow section in the Supporting information, and it starts by defining a double mesa using Cl_2–based inductively-coupled plasma reactive-ion etching (ICP-RIE). The first mesa or junction mesa aims to isolate and protect laterally the QWs, minimizing parasitic etching during the P-ECE. Whereas, the second mesa or device mesa targets to expose the sacrificial layer and access the current spreading layer onto which the electrochemical etching contact is deposited afterward. Then, a 12-pair SiO_2/HfO_2 bottom DBR is sputtered and the bond pads are evaporated on top of the mesa. The bottom DBR also covers the sidewalls of both junction and device mesas protecting against possible parasitic etching in the QWs caused by the P-ECE process and holds the device to the substrate once the sacrificial layer is completely removed. The P-ECE is carried out in a 3 mM HNO_3 electrolyte with an applied bias voltage of 15 V and an illumination of 30 mW/cm^2 from a 275 nm LED. After P-ECE, the devices are bonded to the carrier chip with electroplated Au micropillars, and a HfO_2 spacer layer followed by an 11-pair top DBR are sputtered on the N-face surface of the devices as the sketch of **Figure 1a** shows. The HfO_2 spacer layer refractive index (2.28 at 278.5 nm) is very close to the AlN refractive index (2.27 at 278.5 nm). This allows for placing the N-face in the device in a node of the standing optical field and hence minimizing optical scattering and absorption losses. The total optical cavity length of the VCSELs with a resonance wavelength at 278.5 nm is 2776.3 nm without considering penetration depths into the DBRs.

Prior to the HfO_2 spacer layer and top DBR deposition, the N-face surface of the VCSELs, which was exposed by the P-ECE, was investigated by atomic force microscopy (AFM). The RMS for a 5 × 5 μm^2 scan area was 2.8 nm. This is only 0.7 nm more than the RMS of the as-grown surface of 2.11 nm for a 5 × 5 μm^2 area, and could with optimization likely become as smooth as the as-grown surface, see more details in the Surface Morphology section in the Supporting Information. Figure 1b shows the photoluminescence (PL) spectra and integrated intensity of a VCSEL at different pump power densities. The pump power density is calculated by considering the transmitted pump laser light at 236.5 nm through the top DBR, as the Pump Power Density section in Supporting Information explains. The spectra show a non-linear increase in optical intensity with pump power density around the lasing peak at 278.5 nm. The linewidth narrows down to a full width at half maximum (FWHM) of 21 pm at 4.6 MW/cm^2. The integrated optical intensity spectrum at different pump power densities shows a non-linear optical output power versus pump power density with a clear kink around 3 MW/cm^2 which is thus the threshold pump power (P_{th}), see Figure 1b.

The spectrally-resolved far-field emission pattern below and above the threshold pump power of the VCSEL is shown in **Figure 2a**. Below the threshold at 0.7 × P_{th}, (≈2.1 MW/cm^2), three dispersive parabolic longitudinal modes of the cavity are visible. The separation between the 10λ and 9.5λ cavity modes is 10.9 nm, corresponding well to a 10λ cavity. Above threshold at 1.4 × P_{th}, (≈4.2 MW/cm^2), only one non-dispersive mode, i.e. one lasing mode, is seen at 278.5 nm at the apex of the 10λ parabolic mode. The PL peak of the spontaneous emission of the QWs is

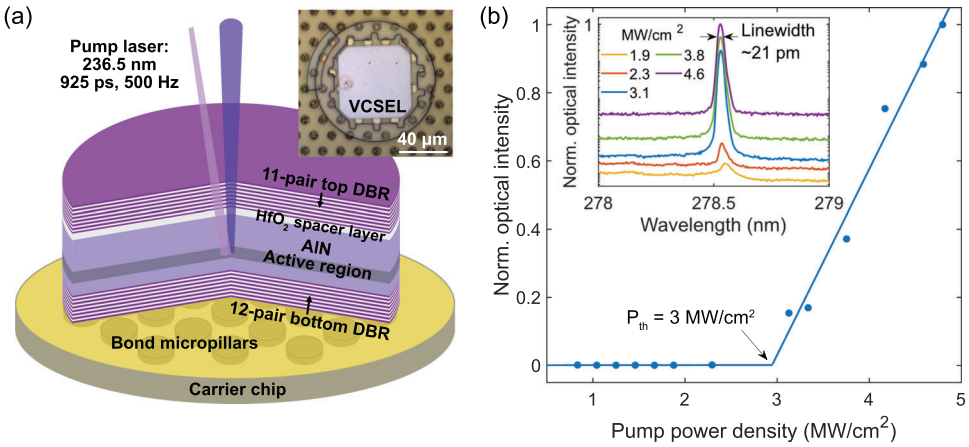

Figure 1. a) Side-view representation and top-view optical microscope image of a VCSEL. b) Optical output power versus pump power density of a VCSEL indicating a threshold pump power density of 3 MW/cm^2. Inset: PL spectra of a VCSEL taken at different pump power densities showing a linewidth around 21 pm at 4.6 MW/cm^2.

276.6 ± 0.2 nm at 4 MW/cm^2 leading to a better spectral overlap between the gain peak and the 10λ cavity mode which increases the modal gain favoring lasing at that longitudinal mode. As can be seen in Figure 2a, the spectrally-resolved far-field above threshold has an angular FWHM of 10°, which is in good agreement with values found in literature for III-Nitride-based VCSELs with ≈2 µm diameter filaments.[18–20] These filaments are in the same order of magnitude as in our devices, see the Filamentation section in the Supporting information.

Figure 2b shows the polarization measurements of surface-emitting light below and above threshold of the VCSEL. The degree of optical polarization has been calculated by the relation $(I_{max} - I_{min}) / (I_{max} + I_{min})$, where I_{max} and I_{min} represent the maximum and minimum normalized optical intensity measured for two orthogonal positions of the polarizer. As can be seen in orange, the in-plane degree of polarization below threshold at 0.85 × P_{th} is ≈11%, indicating the non-polarized nature of the spontaneous emission emitted from the c-plane of the wurzite structure.[21] The small degree of polarization may be due to strain in the QWs,[22] anisotropies in the cavity, or amplified spontaneous emission. In contrast, above threshold at 1.3 × P_{th}, the light is highly linearly polarized with a degree of polarization of ≈87%.

The cavity length control provided by the P-ECE has been studied by measuring several devices across an area of 0.9 × 1.2 mm^2 as the optical microscope image of the devices before bonding in **Figure** 3a shows, where the measured VCSELs are highlighted with a rectangle and its corresponding wavelength and P_{th} are color-coded plotted in Figure 3b. The devices with a designed lasing emission wavelength at 278.5 nm, exhibit a lasing emission wavelength between 277.71 nm to 278.88 nm corresponding to a physical (optical) cavity length difference of 8 nm (≈18 nm) which is less than 1% of the total cavity length. This precise cavity length control is provided by the epitaxial growth and the P-ECE, where

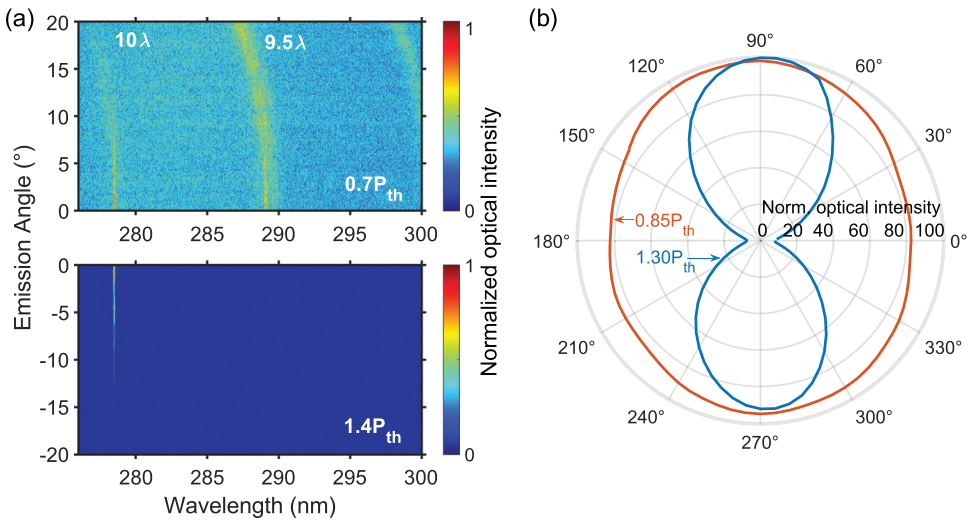

Figure 2. a) Spectrally-resolved far-field emission pattern below (top) and above (bottom) threshold. b) In-plane polarization below (orange) and above (blue) threshold pump power of a VCSEL.

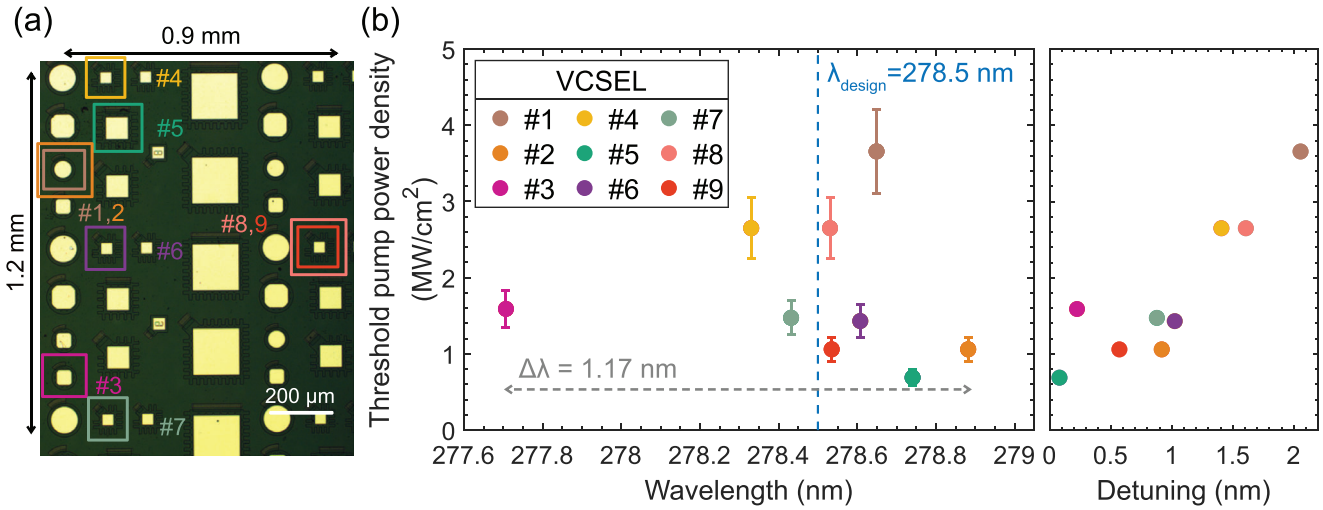

Figure 3. a) Optical microscope image of different devices before bonding over a 0.9 × 1.2 mm² area. Each measured VCSEL is highlighted with a rectangle on the optical microscope image and its corresponding lasing emission wavelength, detuning, and P_{th} are color-coded in b). The vertical dashed lines indicate the targeted lasing emission wavelength and the horizontal dashed line shows the span of lasing wavelengths.

the small variation could be due to the roughness of the as-grown and N-face surface, compositional and thickness variations of the cavity and/or the QWs, and the HfO_2 spacer layer. The threshold pump power varies between the devices from 0.7 MW/cm² to 3.7 MW/cm², and there is a strong correlation between threshold pump power density and detuning as seen in Figure 3 where VCSEL #5 has the lowest theshold (0.7 MW/cm²) with a detuning of 0 nm while VCSEL #1 has the highest threshold (3.7 MW/cm²) with a detuning of 2 nm, in line with what has been observed in UVB VCSELs.[11] The detuning is here defined as the difference between the lasing wavelength and the PL peak of the QWs at the lasing threshold. What is important to include when estimating the detuning is the blue-shift of the PL peak with increasing pump power density, as seen in the spectra in Spontaneous Emission of the Active Region in the Supporting Information. Further investigation is needed to understand why the different VCSELs have different detuning, that in these cases mainly are due to a large spectral difference in material gain spectra.

3. Conclusions

In summary, UVC VCSELs with a cavity length variation of less than 1% within an area of 0.9 × 1.2 mm² have been presented. The VCSELs were fabricated employing P-ECE as substrate removal, allowing to deposit dielectric DBRs on both sides of the cavity. This new methodology allowed the fabrication of membrane devices with an ≈0.72 nm rougher N-face compared to the as-grown surface. Above threshold, the spatially resolved far-field emission pattern shows a non-parabolic narrow lasing line with an angular FWHM of 10° and linear polarization of 87%. The precise cavity length control resulted in a shift of the lasing wavelength only varying 1.17 nm in 0.9 × 1.2 mm², and a threshold power density as low as 0.7 MW/cm² when the detuning is 0 nm. This threshold is comparable to those of early optically pumped GaN-based VCSELs that were between 43 MW/cm² and 0.13 MW/cm².[23] It is also comparable to state-of-the-art UVB VCSELs with a threshold of 0.4 MW/cm²[11] and UVC VCSELs with a threshold of 0.79 MW/cm².[13] It should be noted that comparing thresholds of optically pumped VCSELs is not straightforward since the threshold depends upon pump laser wavelength, transmission of the top DBR at the pump wavelength, pulse length,[24] and VCSEL epitaxial structure. Here, we have demonstrated low threshold pump power densities for UVC VCSELs and the potential of P-ECE as a substrate removal technique for the fabrication of UVC VCSEL with an accurate cavity length control, which is a promising step towards the fabrication of more complex VCSEL structures. Further understanding and optimization of the P-ECE should be done to minimize the added RMS to the as-grown surface and explore its effect in n-doped structures. In addition, other challenges must be addressed such as increasing the electrical injection efficiency by sharper interfaces, increasing the internal quantum efficiency by reducing the dislocation density, developing a low absorptive and highly conductive p-side, and developing schemes for transverse electrical confinement. All together, this will eventually lead to the realization of electrically driven UVC VCSELs.

4. Experimental Section

Epitaxial Growth: The epitaxial structure was grown by metal–organic vapor phase epitaxy using a 3 × 2 inch close-coupled shower head reactor on an AlN template on sapphire.[25] The growth started with a transition layer graded from AlN to $Al_{0.8}Ga_{0.2}N$ for strain management and continued with an $Al_{0.76}Ga_{0.24}N$ buffer layer. Subsequently, a stack of layers for P-ECE lift-off that consists of an n-$Al_{0.76}Ga_{0.24}N$ lateral current spreading layer with a Si concentration of 5 × 10^{17} cm^{-3}, an n-$Al_{0.76}Ga_{0.24}N$ etch block layer with a reduced Si concentration of 2.4 × 10^{17} cm^{-3}, and an 18 nm n-$Al_{0.45}Ga_{0.55}N$ sacrificial layer with a Si concentration to 4 × 10^{19} cm^{-3} were grown. The growth continued with a lower 1000 nm AlN cavity, and an active region composed of two $Al_{0.70}Ga_{0.30}N$ barriers that were 40 nm thick embedding five $Al_{0.40}Ga_{0.60}N$ QWs with a thickness of 2 nm. The QWs were separated by 5 nm thick $Al_{0.70}Ga_{0.30}N$. Finally, a top 75-nm thick AlN layer was grown.

Device Fabrication: The UVC VCSEL fabrication is illustrated in the Process Flow section in the Supporting Information, and it started with the

definition of a double mesa by two dry etch steps using a two-step chlorine-based ICP-RIE[26] process. The junction mesa was 700 nm deep, and the device mesa was 850 nm deep. A V(15 nm)/Al(90 nm)/Ni(20 nm)/Au(120 nm) n-contact stack was e-beam evaporated as electrical contacts for electrochemical etching. Next, a short dip in buffered oxide etch was done prior to the metal deposition. The annealing of the contact was performed at 725 °C for 40 s under a nitrogen atmosphere by rapid thermal processing. A 12-pair SiO_2/HfO_2 bottom DBR was sputtered and has a total thickness of ≈940 nm. The bottom DBR also protected against parasitic electrochemical etching of the active region and held the device to the substrate when the sacrificial layer was etched away by P-ECE. On top of the DBR, an Al mirror, a SiO_2 layer to prevent intermixing, and Ti/Au bond pads were e-beam evaporated. Subsequently, the sacrificial layer and the electrochemical etching contact were exposed after the DBR deposition by ICP-RIE dry etching. For additional protection of the devices during the P-ECE etching, the devices were covered with a 5-µm thick positive photoresist. The P-ECE was performed in a 3 mM HNO_3 electrolyte with an applied bias voltage of 15 V for 20 min. The photo-excitation was done with a 275 nm LED with a power density of 30 mW/cm^2. After stripping the photoresist, the VCSEL membranes were Au–Au thermo-compressibility bonded to a Si carrier chip with pre-defined Au metal pads. A 32 nm HfO_2 spacer layer and 11-pair SiO_2/HfO_2 top DBR were sputtered on the N-face of the devices.

Optical Characterization: PL measurements were performed with a 236.5 nm diode-pumped solid-state (PDSS) laser, which utilizes a fourth harmonic generation of Nd:YAG laser at 946 nm. The DPSS laser has a repetition rate of 500 Hz and a pulse duration of 925 ps. The diameter of the excitation spot (FWHM) was estimated to be ≈10 µm and the measurements were performed at room temperature. The spectrally resolved far-field emission was captured by using a microscope objective with NA = 0.39 for collecting the angular distribution between ±20° and two lenses in the 4f-arrangement to image the Fourier plane on the spectrometer slit, where the angular information was spectrally resolved and imaged on a Peltier-cooled 2048 × 512 pixels charge-coupled device camera. The result is a 2D graph showing the emission intensity versus wavelength and angle. A wire grid polarizer placed on a motorized rotation mount located in the common focal plane of the 4f-arrangement was employed for the polarization measurements.

Supporting Information

Supporting Information is available from the Wiley Online Library or from the author.

Acknowledgements

This work was performed in part at Myfab Chalmers University of Technology, and the project was financially supported by the European Research Council (ERC) under the European Union's Horizon 2020 research and innovation program (grant agreement no. 865622), the Swedish Research Council (2018-00295), and the German Federal Ministry of Education and Research (BMBF) with the "Advanced UV for life" project. The authors thank Sylvia Hagedorn from Ferdinand-Braun-Institute for providing the AlN/Sapphire templates and Praphat Sonka for the operation of the metal-organic vapor phase epitaxy system.

Conflict of Interest

The authors declare no conflict of interest.

Data Availability Statement

The data that support the findings of this study are available from the corresponding author upon reasonable request.

Keywords

AlGaN, electrochemical etching, photo-assisted electrochemical etching, UVC, VCSEL

Received: December 16, 2024
Revised: February 18, 2025
Published online: March 29, 2025

[1] N. Demeersseman, V. Saegeman, V. Cossey, H. Devriese, A. Schuermans, *J. Hosp. Infect.* **2023**, *132*, 85.
[2] J. Hodgkinson, R. P. Tatam, *Meas. Sci. Technol.* **2012**, *24*, 012004.
[3] Y. Watanabe, Y. Kanaya, Y. Saito, T. Sakamoto, K. Masaki, S. Owa, T. Koo, D. Tseng, C. Sorensen, B. Lin, M. Tan, S. Li, S. P. Renwick, N. Hirayanagi, B. Yuan, *J. Micro/Nanopattern., Mater., Metrol.* **2023**, *22*, 041403.
[4] A. Vavoulas, H. G. Sandalidis, N. D. Chatzidiamantis, Z. Xu, G. K. Karagiannidis, *IEEE Commun. Surv. Tutorials* **2019**, *21*, 2111.
[5] R. Michalzik, in *VCSELs: Fundamentals, Technology and Applications of Vertical-Cavity Surface-Emitting Lasers*, (Eds.: R. Michalzik), Springer, Berlin, Heidelberg, **2013**, pp. 19–75. https://doi.org/10.1007/978-3-642-24986-0_2.
[6] A. Babichev, S. Blokhin, E. Kolodeznyi, L. Karachinsky, I. Novikov, A. Egorov, S.-C. Tian, D. Bimberg, *Photonics* **2023**, *10*, 268.
[7] M. Iwaya, S. Tanaka, T. Omori, K. Yamada, R. Hasegawa, M. Shimokawa, A. Yabutani, S. Iwayama, K. Sato, T. Takeuchi, S. Kamiyama, H. Miyake, *Jpn. J. Appl. Phys.* **2022**, *61*, 040501.
[8] Z. Zhang, M. Kushimoto, A. Yoshikawa, K. Aoto, L. J. Schowalter, C. Sasaoka, H. Amano, *Appl. Phys. Express* **2022**, *15*, 041007.
[9] T. Hamaguchi, M. Tanaka, H. Nakajima, *Jpn. J. Appl. Phys.* **2019**, *58*, SC0806.
[10] F. Hjort, J. Enslin, M. Cobet, M. A. Bergmann, J. Gustavsson, T. Kolbe, A. Knauer, F. Nippert, I. Häusler, M. R. Wagner, T. Wernicke, M. Kneissl, Å. Haglund, *ACS Photonics* **2021**, *8*, 135.
[11] G. Cardinali, F. Hjort, N. Prokop, J. Enslin, M. Cobet, M. A. Bergmann, J. Gustavsson, J. Ciers, I. Häusler, T. Kolbe, T. Wernicke, Å. Haglund, M. Kneissl, *Appl. Phys. Lett.* **2022**, *121*, 103501.
[12] Z. Zheng, Y. Mei, H. Long, J. Hoo, S. Guo, Q. Li, L. Ying, Z. Zheng, B. Zhang, *IEEE Electron Device Lett.* **2021**, *42*, 375.
[13] Z. Zheng, Y. Wang, J. Hoo, S. Guo, Y. Mei, H. Long, L. Ying, Z. Zheng, B. Zhang, *Sci. China Mater.* **2023**, *66*, 1978.
[14] M. A. Bergmann, J. Enslin, R. Yapparov, F. Hjort, B. Wickman, S. Marcinkevičius, T. Wernicke, M. Kneissl, Å. Haglund, *Appl. Phys. Lett.* **2019**, *115*, 182103.
[15] Y. Zhang, S.-W. Ryu, C. Yerino, B. Leung, Q. Sun, Q. Song, H. Cao, J. Han, *Phys. Status Solidi B* **2010**, *247*, 1713.
[16] M. A. Bergmann, J. Enslin, M. Guttmann, L. Sulmoni, N. L. Ploch, F. Hjort, T. Kolbe, T. Wernicke, M. Kneissl, Å. Haglund, *ACS Photonics* **2023**, *10*, 368.
[17] E. Torres, J. Ciers, M. A. Bergmann, J. Höpfner, S. Graupeter, M. Grigoletto, M. Guttmann, T. Kolbe, T. Wernicke, M. Kneissl, Å. Haglund, *ACS Photonics* **2024**, *11*, 2923.
[18] T.-C. Lu, J.-R. Chen, S.-W. Chen, H.-C. Kuo, C.-C. Kuo, C.-C. Lee, S.-C. Wang, *IEEE J. Sel. Top. Quantum Electron.* **2009**, *15*, 850.
[19] T.-C. Lu, S.-W. Chen, T.-T. Wu, P.-M. Tu, C.-K. Chen, C.-H. Chen, Z.-Y. Li, H.-C. Kuo, S.-C. Wang, *Appl. Phys. Lett.* **2010**, *97*, 071114.
[20] T.-C. Chang, S.-Y. Kuo, J.-T. Lian, K.-B. Hong, S.-C. Wang, T.-C. Lu, *Appl. Phys. Express* **2017**, *10*, 112101.
[21] M. Kneissl, J. Raß, L. Schade, U. T. Schwarz, in *III-Nitride Based Light Emitting Diodes and Applications*, (Eds.: T.-Y. Seong, J. Han, H. Amano, H. Morkoç), Springer, Singapore **2017**, pp. 93–128. https://doi.org/10.1007/978-981-10-3755-9_5.

[22] S.-H. Park, J. Kim, D. Ahn, E. Yoon, *Physica E* **2020**, *120*, 114112.
[23] H.-c. Yu, Z.-w. Zheng, Y. Mei, R.-b. Xu, J.-p. Liu, H. Yang, B.-p. Zhang, T.-c. Lu, H.-c. Kuo, *Prog. Quantum Electron.* **2018**, *57*, 1.
[24] W. J. Liu, X. L. Hu, L. Y. Ying, S. Q. Chen, J. Y. Zhang, H. Akiyama, Z. P. Cai, B. P. Zhang, *Sci. Rep.* **2015**, *5*, 9600.
[25] S. Hagedorn, S. Walde, A. Knauer, N. Susilo, D. Pacak, L. Cancellara, C. Netzel, A. Mogilatenko, C. Hartmann, T. Wernicke, M. Kneissl, M. Weyers, *Phys. Status Solidi A* **2020**, *217*, 1901022.
[26] H. K. Cho, J. H. Kang, L. Sulmoni, K. Kunkel, J. Rass, N. Susilo, T. Wernicke, S. Einfeldt, M. Kneissl, *Semicond. Sci. Technol.* **2020**, *35*, 095019.